Zhang et al. *Zool. Res.* 2025, 46(6): 1363−1374
https://doi.org/10.24272/j.issn.2095-8137.2025.115
https://cstr.cn/32248.14.zr.2025.115

ZR | Zoological Research

Article Open Access

PMEL as a candidate gene for coat color differentiation in Sibu yaks: Genetic and functional insights

Hao-Yuan Zhang[1,#], Lu Xu[1,#], Jin-Huan Wang[2,#], Simone Ceccobelli[3], Yong Zhu[4], Qiang Zhang[4], Cheng-Fu Zhang[4], Peng-Fei Hu[5], Cheng-Li Liu[1], Bai-Gao Yang[1], Peng-Cheng Ruan[1], Tao Ren[1], He Cong[1], Yan Zeng[1], Yan-Guo Han[1], Shi-Zhi Wang[1], Yong-Ju Zhao[1], Zhong-Quan Zhao[1], Yong-Fu Huang[1], Wen-Hui Nie[2,*], Guang-Xin E[1,*]

[1] *College of Animal Science and Technology*, *Southwest University*, *Chongqing* 400715, *China*
[2] *Kunming Cell Bank*, *Kunming Institute of Zoology*, *Chinese Academy of Sciences*, *Kunming*, *Yunnan* 650223, *China*
[3] *Department of Agricultural*, *Food and Environmental Sciences*, *Università Politecnica delle Marche*, *Ancona* 60131, *Italy*
[4] *Institute of Animal Husbandry and Veterinary Medicine*, *Xizang Academy of Agriculture and Animal Husbandry Science*, *Lhasa*, *Xizang* 850009, *China*
[5] *Institute of Antler Science and Product Technology*, *Changchun Sci-Tech University*, *Changchun*, *Jilin* 130000, *China*

ABSTRACT

Coat color represents a key phenotypic trait in Sibu yak, exhibiting distinct black and brown phenotypes. To elucidate the genetic basis of the brown phenotype, genome-wide association studies and multi-omics analyses were integrated to identify loci and molecular pathways involved in pigmentation. In total, 11 single-nucleotide polymorphisms (SNPs) on chromosome (chr) 5 displayed genome-wide significance (*P*-adjust<4.47×10^{-9}), with the lead variant (chr5: g.47487664 A>G, *P*-adjust=2.38×10^{-10}) located within an intron of *PMEL*. Expression analysis revealed markedly reduced *PMEL* transcription in fibroblasts from brown individuals. Functional multi-omics analyses of *PMEL* overexpression demonstrated significant alteration of the expression of 1 088 genes, 444 proteins, and 57 metabolites. Enrichment analyses indicated significant involvement of melanogenesis-related signaling cascades, including cAMP (e.g., *ADCY7*, EDNRA, and epinephrine), PI3K-Akt (e.g., *FGF5*, *PIK3CG*, and FGF7), and MAPK (e.g., *MAP2K6*, *FGFR3*, and ERBB4) pathways. These findings indicate that the intronic *PMEL* variant modulates gene expression and pigmentation through coordinated regulation of these pathways, thereby contributing to the phenotypic divergence of Sibu yak coat color. This study provides valuable insights into the genetic mechanisms underlying Sibu yak pigmentation and identifies *PMEL* as a key candidate gene governing coat color differentiation in Sibu yak.

Keywords: Yak; Multi-omics; Melanogenesis; Yak fibroblast

INTRODUCTION

The yak (*Bos grunniens*) is an indigenous bovid species native to the Qinghai-Xizang Plateau and adjacent alpine regions, where extreme environmental conditions have exerted strong selective pressures shaping diverse adaptive phenotypes. These pressures have driven genomic and physiological specialization, enabling survival in hypoxic, cold, and ultraviolet-intense environments. Recent advances in comparative genomic and transcriptomic analyses have identified various candidate genes associated with high-altitude adaptation (Ji et al., 2021; Wang et al., 2020), growth performance (Ji et al., 2021), rib number variation (Lan et al., 2021), and hematological traits (Ma et al., 2019). In the context of pigmentation, mutations in *MC1R* (p.Gln34*, p.Met73Leu, and p.Arg142Pro) and *PMEL* (p.Leu18del) have been associated with the brown coat phenotype (Zhang et al., 2014), while *KIT*-related Cs alleles have been implicated in the white phenotype of yaks (Zhang et al., 2014, 2023). Despite these findings, the molecular and regulatory mechanisms governing coat color variation remain poorly resolved. Given the importance of coat color as an adaptive trait in high-altitude environments, elucidating its genetic and molecular bases is of considerable evolutionary and biological importance.

Pigmentation is a highly coordinated, complex biological process involving pigment cell specification, migration,

Received: 11 August 2025; Accepted: 15 September 2025; Online: 16 September 2025

Foundation items: This work was supported by the Research and Integrated Demonstration of Efficient Breeding Technology for Yaks (XZ202101ZD0002N-02) and Fundamental Research Funds for the Central University (SWU-XDJH202301)

[#]Authors contributed equally to this work

*Corresponding authors, E-mail: whnie@mail.kiz.ac.cn; eguangxin@126.com

differentiation, and melanin synthesis (Caro & Mallarino, 2020; Cieslak et al., 2011). Melanin, the principal pigment determining coat coloration in mammals, plays critical roles in protection against ultraviolet radiation and in thermoregulation (Le et al., 2021; Weiner et al., 2014). During embryogenesis, neural crest cells differentiate into melanoblasts, which migrate to target tissues and mature into melanin-producing melanocytes (Bonaventure et al., 2013). Within melanocytes, melanin synthesis occurs in specialized organelles known as melanosomes. Tyrosine is first converted by tyrosinase into L-3,4-dihydroxyphenylalanine (DOPA), which is oxidized to dopaquinone, the precursor for eumelanin and pheomelanin biosynthesis (Wasmeier et al., 2006; Weiner et al., 2014). Finally, melanin is transferred to keratinocytes via melanosomes, resulting in pigment deposition across the epidermis (Lambert et al., 2019). Although the developmental and biochemical mechanisms of melanogenesis have been extensively characterized, the genetic networks and regulatory hierarchies orchestrating pigmentation in yak remain insufficiently understood.

More than 650 genes have been implicated in pigmentation (Baxter et al., 2019), many contributing to the diversity of coat color phenotypes observed across domestic species. Among them, the melanocortin 1 receptor (*MC1R*), a seven-transmembrane G protein-coupled receptor, plays a central role in regulating melanin synthesis (Mun et al., 2023). Functional mutations in *MC1R* have been shown to modulate melanogenesis, resulting in coat color variation in cattle (He et al., 2022), pigs (Dun et al., 2007), goats (Fontanesi et al., 2009), and sheep (Yang et al., 2013). The agouti signaling protein (*ASIP*) gene acts as an endogenous antagonist of *MC1R* (Zhang et al., 2016), inhibiting the binding of α-melanocyte-stimulating hormone (α-MSH) and thereby shifting pigment synthesis from eumelanin to pheomelanin (Voisey & Van Daal, 2002). Mutations in *ASIP* have been associated with extensive variation in coat color patterns among domestic species (Guo et al., 2022; Norris & Whan, 2008; Trigo et al., 2021). Other pigmentation-related genes, such as the KIT proto-oncogene receptor tyrosine kinase (*KIT*), have been associated with different white coat patterns in domestic animals (Fontanesi et al., 2010a, 2010b), whereas a candidate mutation (c.1484_1489del) in tyrosinase-related protein 1 (*TYRP1*) has shown a strong correlation with the brown coat phenotype in Chinese pigs (Ren et al., 2011).

The *PMEL* gene encodes the premelanosome protein, a critical structural component required for the assembly of luminal fibrils within melanocytes (Sun et al., 2018). These fibrils provide a scaffold for the ordered polymerization of highly reactive eumelanin intermediates, ensuring efficient pigment deposition during melanosome maturation (Hellström et al., 2011). Mutations in *PMEL*, including p.Leu18del, Arg625Cys, and SINE insertion, have been linked to partial or complete pigment dilution in multiple species, including mice (Kwon et al., 1995), cattle (Kimura et al., 2022; Wang et al., 2023), yaks (Zhang et al., 2014), horses (Andersson et al., 2013; Brunberg et al., 2006), and dogs (Ballif et al., 2018). Despite extensive progress in elucidating pigmentation genetics, the molecular determinants governing coat color differentiation in high-altitude mammals remain insufficiently characterized, underscoring the need for further investigation using appropriate, physiologically relevant models.

The Sibu yak, an iconic breed inhabiting the Qinghai-Xizang Plateau, exhibits two stable coat color phenotypes—black and brown—shaped by long-term natural selection. This breed represents an exceptional natural model for exploring the genetic and evolutionary mechanisms underlying pigmentation adaptation at high altitude. The present study explored the genetic architecture driving brown and black coat phenotypes in Sibu yak, emphasizing the potential regulatory contribution of *PMEL* to pigmentation diversity.

MATERIALS AND METHODS

All procedures involving animals strictly followed international, national, and institutional guidelines for the ethical care and use of animals. Animal collection procedures complied with the current laws of China, and all experimental protocols were reviewed and approved by the Institutional Animal Care and Use Committee (IACUC) of Southwest University (Permit No. IACUC-20190815-04), in accordance with the recommendations of the Regulations for the Administration of Affairs Concerning Experimental Animals of China.

Genome sequencing and genome-wide association studies (GWAS)

Blood samples were collected from black Sibu yaks (*n*=30) and brown Sibu yaks (*n*=50) (Supplementary Table S1) in Mozhugongka County, Lhasa City, Xizang (altitude >3 800 m a.s.l., N29°61'61" and E91°74'64"). Whole-blood samples were collected via jugular venipuncture into EDTA anticoagulant tubes (Becton, Dickinson and Company, USA). Genomic DNA was immediately extracted using the MiniBEST Universal Genomic DNA Extraction Kit v.5.0 (Takara, Japan). Sequencing libraries were prepared with the Annoroad® Universal DNA Library Prep Kit v.2.0 (Illumina®, USA) and sequenced on the BGI DNBSEQ-T7 platform (Beijing Genomics Institution, China).

Raw reads were processed using Fastp v.0.20.0 (https://github.com/OpenGene/fastp) to obtain high-quality reads. Clean reads were aligned to the LU_Bosgru_v3.0 (GCA_005887515.1) reference genome using BWA-MEM2 (https://github.com/bwa-mem2/bwa-mem2). Polymerase chain reaction (PCR) duplicates were removed using Sambamba v.0.6.6 (https://github.com/biod/sambamba). Single-nucleotide polymorphisms (SNPs) were identified and filtered with GATK v.4.2.4.1 and subsequent quality control was conducted using PLINK v.1.90 (https://www.cog-genomics.org/plink/1.9/), excluding loci with minor allele frequency <0.05 and a call rate <90%.

Genome-wide association analysis of all 80 individuals was performed to identify candidate genes regulating coat color, using GCTA v.1.94.1 (https://yanglab.westlake.edu.cn/software/gcta/#fastGWA-GLMM) based on a generalized linear mixed model:

$$\text{logit}(\text{"}\mu) = x_s\beta_s + X_c\text{"}\beta_c + g \quad (1)$$

where μ represents the vector of probabilities ($\mu_i = P(y_i = 1|x_{si}, X_{ci}, g_i)$), and individual *i* corresponds to the case phenotype (brown coat color); x_s denotes the genotype dosage for the SNP under test, with its fixed effect indicated by β_s; X_c is the matrix of covariates, and β_c represents their corresponding effect sizes; g is the vector of random polygenic effects capturing background genetic variation and relatedness, estimated via the genetic relationship matrix (Jiang et al., 2021). The significance threshold was set at 0.05/*N*, where *N* represents the number of SNPs. Kyoto Encyclopedia of Genes and Genomes (KEGG) and Gene

Ontology (GO) analyses of candidate genes were visualized using KOBAS (http://kobas.cbi.pku.edu.cn/).

Validation of key SNP and analysis of *PMEL* expression

Blood samples were obtained from 169 Sibu yaks (50 black and 119 brown), and genomic DNA was extracted for variant validation. A primer pair targeting the *PMEL* locus on chromosome 5 (chr5: g.47487664 A>G) was designed using the Primer3 online tool (https://primer3.ut.ee/). The primer sequences were: forward 5'-TTGGTCTACGTCATGGAGGG-3' and reverse 5'-ACACGTACCAGACACACAGT-3'. PCR amplification was performed using the Takara PCR Amplification Kit (Japan) under the following conditions: initial denaturation at 95℃ for 5 min, followed by 35 cycles of denaturation at 95℃ for 30 s, annealing at 56℃ for 30 s, extension at 72℃ for 30 s, and final extension at 72℃ for 5 min. The PCR products were subjected to Sanger sequencing using the ABI 3730 DNA Analyzer (Life Technologies, USA), and sequencing results were visualized using Chromas v.2.6.6 (https://technelysium.com.au).

Fibroblasts derived from black and brown Sibu yak were provided by the Institute of Animal Science, Chinese Academy of Agricultural Sciences. Genomic DNA extracted from these yak fibroblasts (YFs) was used for SNP validation via PCR amplification and Sanger sequencing of the chr5: g.47487664 A>G locus. Total RNA from the same cells was isolated using the MiniBEST Universal RNA Extraction Kit (Takara, Japan). Transcriptional expression differences in *PMEL* expression between black and brown YFs were compared using reverse transcription quantitative PCR (RT-qPCR), with glyceraldehyde 3-phosphate dehydrogenase (*GAPDH*) used as the housekeeping gene.

Cell culture and stable transfection construction

The YF line, derived from ear tissue, was obtained from the Kunming Cell Bank, Chinese Academy of Sciences (National Science and Technology Infrastructure, National Biomedical Cell-Line Resource, NSTI-BMCR). Cells were maintained in complete medium consisting of 89% Dulbecco's Modified Eagle Medium/Nutrient Mixture F-12 (DMEM/F-12, Thermo Scientific, USA), 10% fetal bovine serum (Thermo Scientific, USA), and 1% penicillin/streptomycin (Thermo Scientific, USA) in an incubator (Forma Series 3, Thermo Scientific, USA) at 37℃ with 5% CO_2. The medium was changed every 2 days. When the YFs reached 80%–90% confluence, subculturing was performed at a 1:2 ratio.

The full-length coding sequence of *PMEL*, synthesized according to the GenBank reference (Gene ID: 102277998), was subcloned into the vector pHBLV-CMV-MCS-3FLAG-EF1-ZsGreen-T2A-PURO under the control of the CMV promoter using BamHI and EcoRI restriction enzymes (Thermo Scientific, USA), generating the final recombinant plasmid (HBLV-b-PMEL-3xflag-ZsGreen-PURO). The target fragment was amplified by PCR using the primers forward 5'-TACTAGAGGATCTATTTCCGGTGAATTCGCCACCATGGATCTGGTGCT-3' and reverse 5'-GTCACTTAAGCTTGGTACCGAGGATCCGACCTGCTGTCCACTGAGGA-3'. Lentiviral packaging and quality testing were carried out by the HANBIO Company (China). *PMEL*-overexpressing YFs were generated by transducing cells at 30%–50% confluence with the transfection reagent polybrene and diluted lentivirus. Transduction efficiency was assessed 48–72 h post-infection using a fluorescence microscope (Leica, Germany). When infection efficiency exceeded 80% and cell confluence reached 60%–70%, puromycin (10 μg/mL) was added for 48 h to select stably transduced cells. *PMEL* expression was confirmed via RT-qPCR, with *GAPDH* used as the housekeeping gene.

Stable *PMEL*-overexpressing YFs were digested and seeded into 6-well plates. Cells were collected when confluence exceeded 90%. Four biological replicates were prepared for each group—*PMEL*-overexpressing and negative control (NC)—for downstream transcriptomic, proteomic, and metabolomic analyses.

Total RNA extraction and transcriptomic analysis

Total RNA was extracted from each cell group using the MiniBEST Universal RNA Extraction Kit (Takara, Japan). RNA quality was assessed using a NanoDrop™ One spectrophotometer (NanoDrop Technologies, USA). Ribosomal RNA was removed using a Takara Clontech RiboGone Kit (Japan). RNA sequencing (RNA-seq) libraries were generated using the NEBNext Ultra Directional RNA Library Prep Kit for Illumina (NEB, USA), followed by sequencing on the Illumina NovaSeq 6000 platform (Illumina®, USA).

High-quality clean data were obtained using fastp v.0.20.0 (https://github.com/OpenGene/fastp). Ribosomal RNA reads were filtered using Bowtie v.2.3.5.1 (https://bowtie-bio.sourceforge.net/bowtie2/index.shtml). High-quality clean reads were then aligned to the domestic yak reference genome LU_Bosgru_v3.0 (GCA_005887515.1) using HISAT2 v.2.1.0 (https://daehwankimlab.github.io/hisat2/). Transcript assembly and quantification were performed using StringTie v.2.1.1 (https://github.com/gpertea/stringtie), and expression levels were normalized as fragments per kilobase of transcript per million mapped reads (FPKM). Principal component analysis (PCA) was performed using the *prcomp* function in R (www.r-project.org). Differentially expressed genes (DEGs) were identified using DESeq2 (https://github.com/thelovelab/DESeq2), with a false discovery rate (FDR)<0.05 and $|\log_2$ fold change (FC)|≥1. Functional enrichment of DEGs was evaluated through KEGG and GO analyses using KOBAS (http://kobas.cbi.pku.edu.cn/), with the significance threshold set to adjusted P<0.05.

Total protein extraction and proteomic analysis

Each cell sample was lysed in buffer containing 8 mol/L urea, 1 mmol/L PMSF, and 2 mmol/L EDTA, incubated for 5 min, and sonicated on ice for an additional 5 min. The lysate was centrifuged at 15 000 ×g for 10 min at 4℃, and the supernatant was collected. Protein desalting and enzymatic digestion with trypsin were performed according to previously described methods (Sun et al., 2023). Total protein concentration was measured using a BCA Protein Assay Kit (Beyotime, China).

Proteomic profiling was conducted using 4D label-free technology, which incorporates ion mobility as the fourth analytical dimension alongside retention time, mass ratio (m/z), and ion strength. Protein identification and quantification were carried out by MetWare Biotechnology (China) using a NanoElute efficient liquid phase spectrometer (Bruker Daltonics, Germany) and the timsTOF Pro2 mass platform (Bruker Daltonics, Germany). Raw data were analyzed with DIA-NN v.1.8.1 using a library-free approach based on the domestic yak genome. The LU_Bosgru_v3.0.pep.all.fasta database was used to generate a spectral library for protein quantity analysis. The FDRs for both the protein and precursor

ion levels were maintained below 1%. Relative protein abundance was calculated using the MaxLFQ algorithm implemented in DIA-NN (Cox et al., 2014). The relative quantitative value of each protein across samples was calculated as $R_{ij} = I_{ij} / Median(I_i)$, where *i* represents the sample and *j* denotes the protein. Proteins with FC≥1.5/FC≤0.6667 and *P*<0.05 between comparison groups were defined as differentially expressed proteins (DEPs). Functional enrichment analyses, including KEGG and GO, were conducted using KOBAS (http://kobas.cbi.pku.edu.cn/), applying an adjusted *P*<0.05 as the threshold for significant enrichment.

Metabolomic analysis

For metabolomic profiling, cell samples were analyzed by MetWare Biotechnology using the AB Sciex QTRAP 6500 Liquid Chromatography-Tandem Mass Spectrometry (LC-MS/MS) platform. Data acquisition and quantification were conducted with Analyst v.1.6.3 and MultiQuant v.3.0.3, respectively. PCA was carried out using the function *prcomp* within R (www.r-project.org). Pearson correlation coefficients (PCCs) between samples were calculated using the *cor* function in R. Hierarchical clustering and correlation heatmaps were generated using the ComplexHeatmap package in R.

Metabolic annotation and pathway mapping were performed using the KEGG (https://www.genome.jp/kegg/), HMDB (https://hmdb.ca/), and CHEBI (https://www.ebi.ac.uk/chebi/aboutChebiForward.do) databases. Differentially expressed metabolites (DEMs) were defined by variable importance in projection (VIP)>1 ($|Log_2FC|≥1$) and *P*<0.05 (Student's *t*-test). VIP values were extracted from OPLS-DA models constructed using the MetaboAnalystR package in R. Candidate metabolites were annotated using the KEGG compound (http://www.kegg.jp/kegg/compound/) and pathway (http://www.kegg.jp/kegg/pathway.html) databases. Significant enrichment was defined as *P*-adjust<0.05.

Multiomics integration analysis

PCCs between transcriptomic, proteomic, and metabolomic datasets were calculated using the cor function in R (https://www.r-project.org/). Significant correlations among DEGs, DEPs, and DEMs were defined as |PCC|>0.8 and *P*<0.05.

Reverse transcription quantitative PCR validation of transcriptomic data

Validation of RNA-seq expression profiles was performed using the CFX96-Touch™ Real-Time PCR Detection system (Bio-Rad, USA). The same RNA samples used for RT-qPCR were used for RNA-seq. cDNA was synthesized using the PrimeScript™ RT Reagent Kit with gDNA Eraser (Takara, Japan). Primer sequences for target genes are listed in Supplementary Table S2.

The qPCR mixture (25 μL) included 12.5 μL of TB Green Premix Ex Taq II (Tli RNaseH Plus, 2×) (Takara, Japan), 2.0 μL of cDNA solution, 1.0 μL (10 μmol/L) of each primer, and 8.5 μL of ddH_2O. The qPCR amplification system consisted of an initial denaturation at 95℃ for 30 s, followed by 40 cycles at 95℃ for 5 s and 60℃ for 30 s. Each qPCR run was repeated at least three times. *GAPDH* was used as the housekeeping gene to normalize gene expression, and relative mRNA expression was calculated using the $2^{-\Delta\Delta Ct}$ method, with statistical significance defined as *P*<0.05.

RESULTS

A total of 1 117.23 Gb of genomic data were generated from 80 Sibu yaks, with sequencing depth ranging from 4.87× to 11.54× across individuals (Supplementary Table S3). After quality filtering, 11 188 559 SNPs were identified. The GWAS results identified 11 significant SNPs on chr5 that exceeded the Bonferroni significance threshold (P-adjust<4.47×10^{-9}) (Figure 1C; Supplementary Table S4). Nine genes were annotated from these significant loci, which were enriched in 36 KEGG pathways and 169 GO terms (Supplementary Tables S5, S6). Among them, 10 KEGG pathways, including the PI3K-Akt signaling pathway, ErbB signaling pathway, and metabolic pathways, and 101 GO terms, including protein binding, melanosome organization, and protein domain-specific binding, were significantly enriched (*P*-adjust<0.05). Notably, *PMEL* was significantly enriched in GO categories associated with melanin biosynthetic process, melanosome, and melanosome organization. The most significant SNP (chr5: g.47487664 A>G, P-adjust=2.38×10^{-10}) was located within the intron of *PMEL*. Genotype analysis indicated that all black yaks were A/A homozygotes, whereas most brown yaks (81.82%) were A/G heterozygotes or G/G homozygotes (Supplementary Tables S7, S8).

Genotyping of 169 Sibu yaks further confirmed that all black individuals carried the A/A genotype, while 83.19% of brown yaks were A/G heterozygotes and 16.81% were A/A homozygotes (Supplementary Tables S7, S8). These results were consistent with those derived from whole-genome sequencing, validating the reliability of the GWAS findings.

Sanger sequencing verified the presence of heterozygous mutations (A/G) at chr5_47487664 in brown Sibu YFs (Figure 1C). Significantly higher *PMEL* expression was observed in black YFs (chr5: g.47487664, A/A) compared with brown YFs (chr5: g.47487664, A/G) (*P*<0.001; Figure 1D).

Cell transfection experiments confirmed successful and stable overexpression of the *PMEL* plasmid in YFs (Figure 2A, B). Furthermore, *PMEL* expression in *PMEL*-overexpressing group was significantly higher than in the NC group. Transcriptome sequencing of eight samples produced a total of 78.43 Gb of clean data, with each sample yielding approximately 8 Gb and Q30 scores exceeding 95% (Supplementary Table S9). More than 70% of the high-quality reads were successfully mapped to the reference genome.

A total of 14 415 mRNAs were identified, including 12 197 annotated genes from the ENSEMBL genome browser (www.ensembl.org/) and 2 218 novel genes. PCA of the expression matrix (Figure 2C) revealed clear separation between the *PMEL*-overexpressing and NC groups, indicating substantial genetic divergence. Comparative analysis identified 1 088 DEGs, including 448 up-regulated and 640 down-regulated transcripts in the *PMEL*-overexpressing cells (Figure 2D; Supplementary Table S10). KEGG enrichment analysis revealed that the DEGs were significantly enriched in three pathways—NOD-like receptor signaling pathway, TNF signaling pathway, and pathways in cancer (Figure 2F; Supplementary Table S11). Interestingly, 11 DEGs, including adenylate cyclase 4 (*ADCY4*), adenylate cyclase 7 (*ADCY7*), and endothelin-1 (*EDN1*), were related to melanogenesis and melanoma. Several DEGs were also enriched in pathways associated with the regulation of melanogenesis, including the cAMP, PI3K-Akt, and MAPK signaling pathways. GO enrichment analysis identified 5 857 functional categories, of which 531 were significantly enriched (*P*-adjust<0.05)

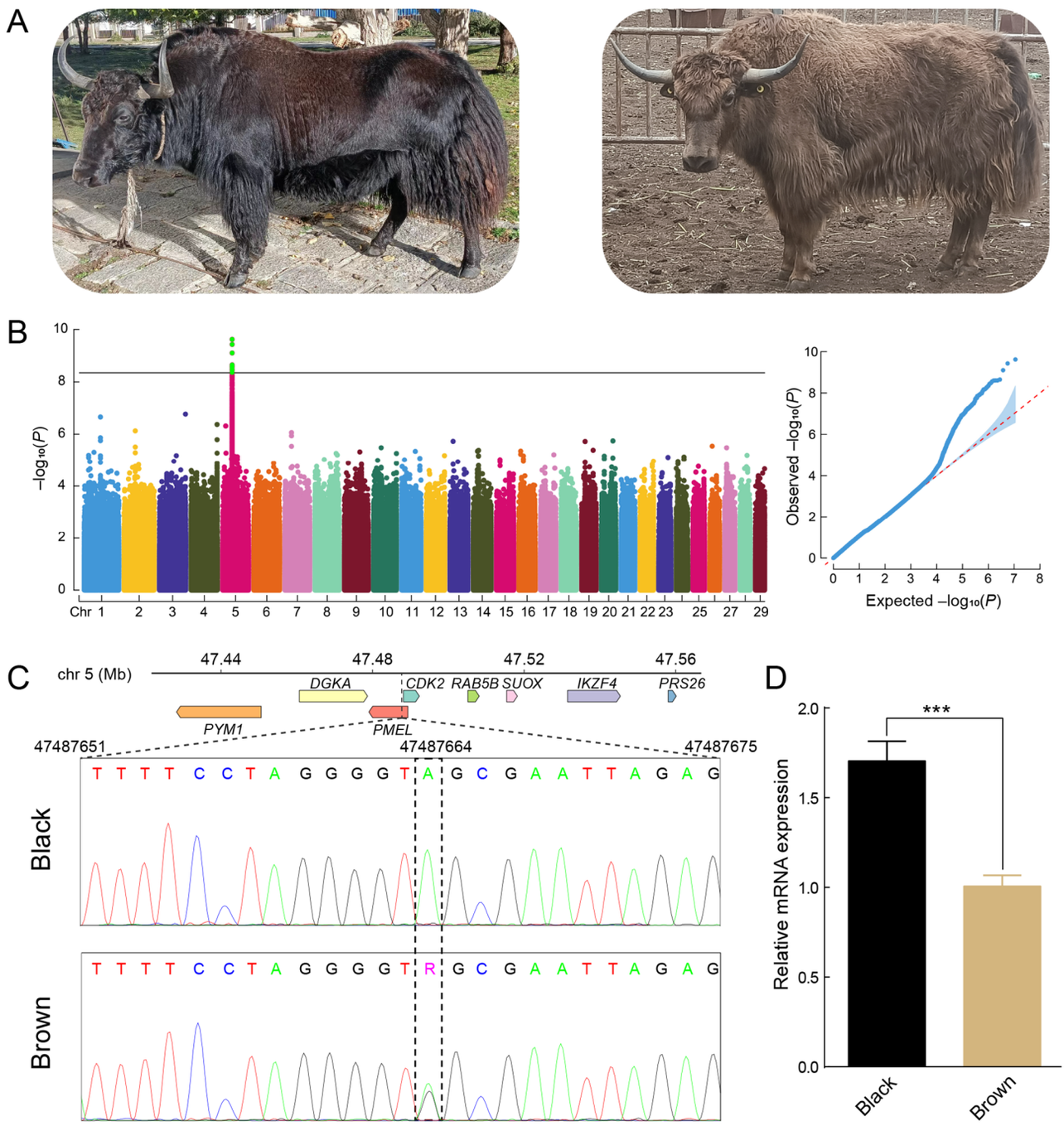

Figure 1 Genome-wide association studies of yak coat color

A: Coat color phenotypes of black and brown Sibu yaks. Photos by Yong Zhu. B: Manhattan plot of all autosomal SNPs and quantile-quantile plot comparing observed and expected values. C: Sanger sequencing results of heterozygous mutations at the most significant SNP. Degenerate base R represents a heterozygous site containing adenine (A) and guanine (G), according to the IUPAC degenerate nucleotide codes. D: Comparison of *PMEL* expression between black and brown yak fibroblasts. Results are presented as mean±SEM, ***: P<0.001.

(Figure 2G; Supplementary Table S12). These included multiple terms associated with melanosome assembly, pigment biosynthesis, and melanocyte differentiation, encompassing DEGs such as *EDNRA*, *RAB38*, and *OCA2*. RT-qPCR validation confirmed that the expression profiles of 16 representative DEGs were consistent with the RNA-seq results (Figure 2E). Notably, numerous well-characterized genes involved in melanogenesis exhibited significant differential expression between the groups based on RNA-seq FPKM values (Figure 2H).

Proteomic profiling identified 8 212 proteins across all samples. PCA revealed distinct protein expression patterns between the two groups (Figure 3A). In total, 444 DEPs were detected, including 207 up-regulated and 237 down-regulated in *PMEL*-overexpressing cells relative to the NC group (Figure 3B; Supplementary Table S13). KEGG analysis identified 282 enriched pathways, with 17 showing significant enrichment, including ECM-receptor interaction, cytokine-cytokine receptor interaction, and NOD-like receptor signaling (Figure 3C; Supplementary Table S14). Although no pathway directly associated with pigmentation reached significance, several DEPs, including FGF7, ADCY7, and CALML4, were

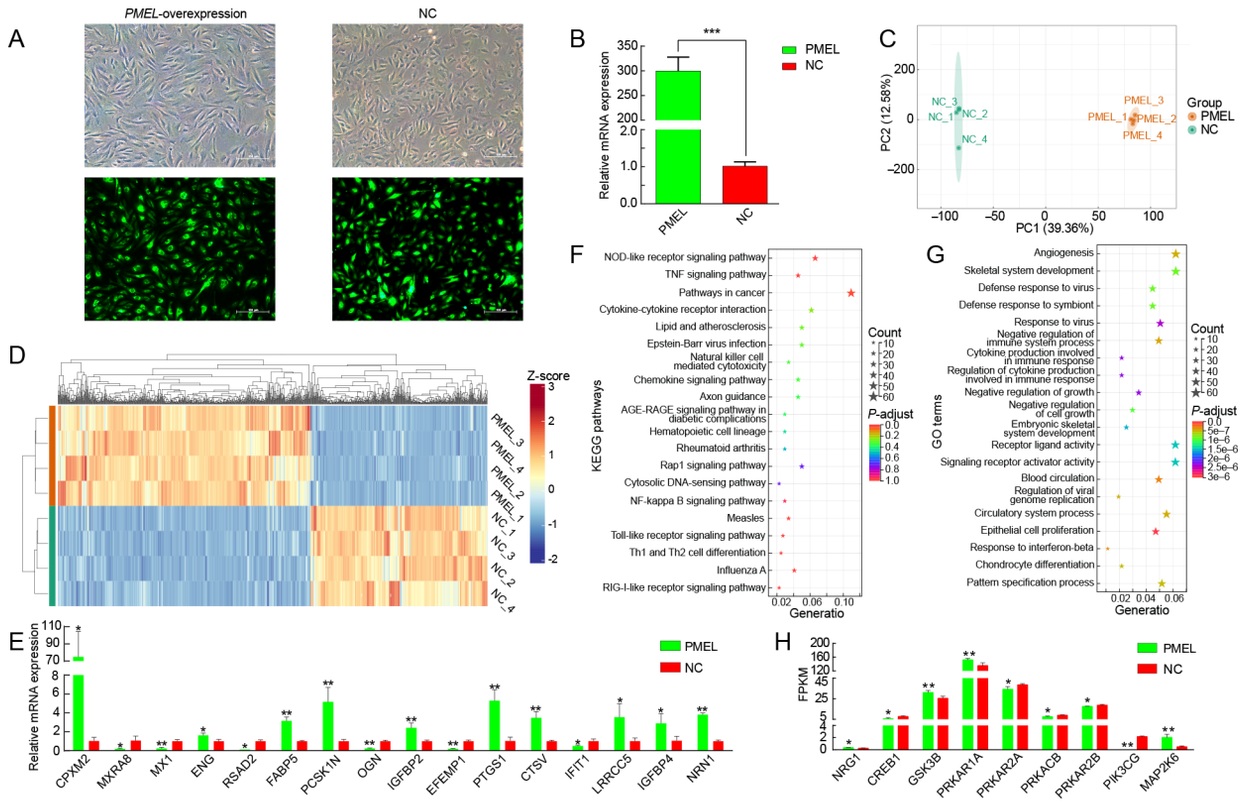

Figure 2 Transcriptional regulatory network of *PMEL* overexpression in yak fibroblasts (YFs) analyzed by RNA-seq

A: Schematic of lentivirus-mediated *PMEL* overexpression in YFs. Scale bars: 100 μm. B: Validation of *PMEL* overexpression efficiency in YFs. C: PCA plot of all samples based on gene expression patterns from RNA-seq. D: Heatmap of differentially expressed genes (DEGs) between *PMEL*-overexpressing and negative control (NC) groups. E: Validation of DEG expression trends from RNA-seq using reverse transcription quantitative PCR. F: Top 20 KEGG pathways enriched by DEGs. G: Top 20 GO terms enriched by DEGs. H: Fragments per kilobase of transcript per million mapped reads of multiple genes associated with melanogenesis regulation in RNA-seq. Results are presented as mean±SEM, *: P<0.05; **: P<0.01; ***: P<0.001.

enriched in the melanoma and melanogenesis pathways. Moreover, ADCY7, FGF7, and ERBB4 were enriched in the cAMP, PI3K-Akt, and MAPK signaling pathways, indicating potential roles in PMEL-mediated pigment regulation.

GO enrichment analysis identified 407 DEPs distributed across 2 450 GO terms. Most terms (67.84%) belonged to the biological process category, including 26 significantly enriched terms (Figure 3D; Supplementary Table S15). Several DEPs were enriched in pigmentation-related functions, including melanosome, pigment cell differentiation, and pigment cell development, suggesting their potential involvement in pigmentation processes.

Integrative correlation analysis of transcriptomic and proteomic data showed that 1 088 DEGs and 444 DEPs were co-enriched in 271 KEGG pathways and 1 448 GO terms. In total, 180 genes displayed concordant differential expression at both mRNA and protein levels (Figure 3E). Significant correlations (|R|>0.8, P<0.05) were observed between multiple DEGs (e.g., *ADCY4*, *ADCY7*, and *FGF5*) and DEPs (e.g., FGF7, ADCY7, and CALML4) co-enriched in melanin-related pathways, melanoma, and melanogenesis (Figure 3F). Additionally, GO categories related to pigmentation, such as pigment cell development, melanin metabolic process, and collagen-activated tyrosine kinase receptor signaling, were significantly enriched (Supplementary Tables S16, S17). Notably, 10 GO terms, including developmental pigmentation, melanosome, and protein tyrosine kinase activity, were co-enriched across both transcriptomic and proteomic datasets (Figure 3G).

A total of 174 metabolites were identified through metabolomic analysis, providing a comprehensive overview of metabolic variations between groups. PCA based on the PLS-DA algorithm revealed highly consistent metabolite expression patterns within each group (Figure 4A). Comparative analysis identified 57 DEMs, including six up-regulated and 51 down-regulated in YFs (Figure 4B; Supplementary Table S18). Notably, metabolites such as N-acetylputrescine, citric acid, 2-picolinic acid, Phe-Leu, H-Phe-Trp-OH, and guanidinoacetic acid exhibited the most pronounced differences in abundance between groups. Based on enrichment analysis, 35 DEMs were enriched in 83 KEGG pathways, including the cAMP signaling, tyrosine metabolism, and ABC transporter pathways (Figure 4C; Supplementary Table S19).

Integrated multi-omics analysis revealed that 180 DEGs, 107 DEPs, and 31 DEMs were co-enriched across 60 KEGG pathways, including salivary secretion, calcium signaling, and Chagas disease (Figure 4D; Supplementary Table S20). Among these, the cAMP signaling pathway was prominently enriched by multiple DEGs (e.g., *EDNRA*, *ADCY7*, and *ADCY4*), DEPs (e.g., ADCY7, EDNRA, and JUN), and DEMs (epinephrine and acetylcholine).

Cross-omics correlation analysis revealed strong concordance in expression trends between DEGs and DEPs involved in the cAMP signaling pathway (Figure 4E). Furthermore, epinephrine and acetylcholine exhibited significant correlations with the expression of several key

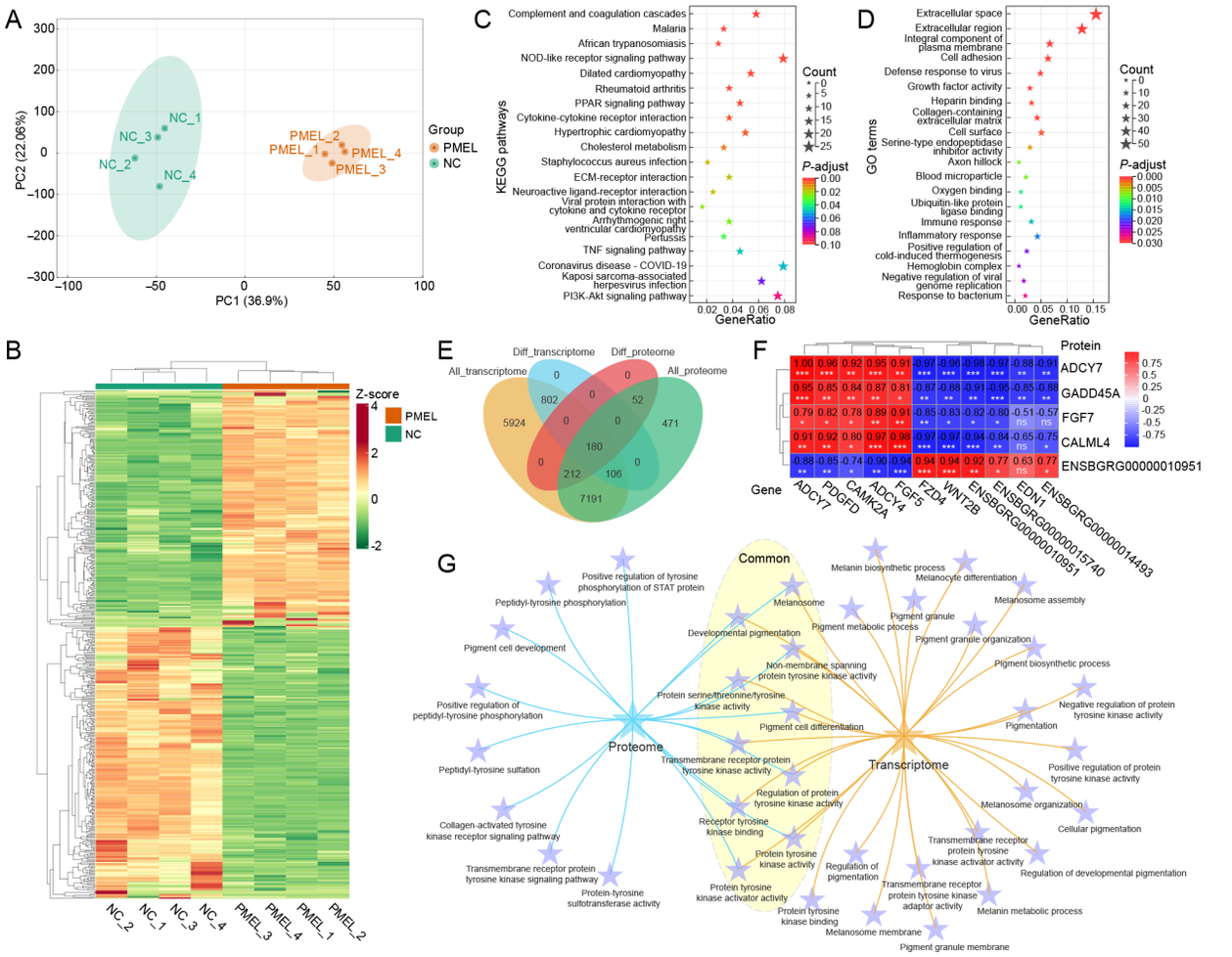

Figure 3 Proteomic regulatory network of *PMEL* overexpression in yak fibroblasts (YFs)

A: PCA plot of samples from different groups. B: Heatmap of differentially expressed proteins (DEPs) between groups. C: Top 20 KEGG pathways enriched by DEPs. D: Top 20 GO terms enriched by DEPs. E: Venn diagram of overlapping differentially expressed genes (DEGs) and DEPs. F: Correlation analysis of melanin-related DEGs and DEPs. G: Intersecting GO terms significantly enriched among both DEGs and DEPs. ns: Not significant; *: P<0.05; **: P<0.01; ***: P<0.001.

DEGs (e.g., *POMC*, *ADCY4*, and *ADCY7*) and DEPs (e.g., ADCY7, EDNRA, and CALML4), highlighting their coordinated regulation within this signaling network (Figure 4E).

DISCUSSION

Genome-wide association analysis identified several candidate genes linked to coat color in yak, highlighting molecular pathways involved in pigmentation and melanocyte regulation. Among these, cyclin-dependent kinase 2 (*CDK2*) encodes a cyclin-dependent kinase regulated by the melanocyte-inducing transcription factor (*MITF*) and is known to promote melanoma cell proliferation (Du et al., 2004). Similarly, *RAB5B* participates in the endocytic uptake and intracellular trafficking of melanocores in epidermal keratinocytes, contributing to pigment transfer and distribution (Correia et al., 2018; Hu et al., 2023). *ERBB3*, a receptor tyrosine kinase implicated in metabolic and pigmentation networks (Edea et al., 2018), functions within a signaling cascade that suppresses melanocyte differentiation and melanin synthesis (Buac et al., 2009), suggesting a potential modulatory role in coat color formation.

A key discovery of this study was the identification of an SNP within the intronic region of *PMEL*, a locus strongly associated with yak coat color. *PMEL* encodes the premelanosome protein, a critical structural component required for the assembly of luminal fibrils within developing melanosomes (Sun et al., 2018). These fibrils protect melanocytes from endogenous toxicity during melanogenesis (Bissig et al., 2016) and accelerate melanogenesis (Fowler et al., 2006). Previous studies have reported that *PMEL* mutations are correlated with the brown coat phenotype in yaks (Zhang et al., 2014), consistent with the current findings. Transcriptomic profiling of white and black yak skin has likewise revealed significant differential expression of *PMEL* (Zhang et al., 2023), reinforcing its pivotal role in pigmentation diversity.

Intronic variants can exert profound regulatory effects by altering cis-regulatory elements, including enhancers, silencers, and splicing motifs (Larsen et al., 2019; Ward & Kellis, 2012). Such mutations may reshape chromatin conformation, alter transcription factor or RNA-binding protein affinity (Fullard et al., 2017; Guo et al., 2003), and perturb long-range chromatin interactions essential for gene activation (Visser et al., 2015). Increasing evidence indicates that intronic polymorphisms can significantly influence transcriptional activity (Grabski et al., 2021; Shaul, 2017; Xiang et al., 2018). The observed differential expression of *PMEL* between black and brown YFs therefore supports the

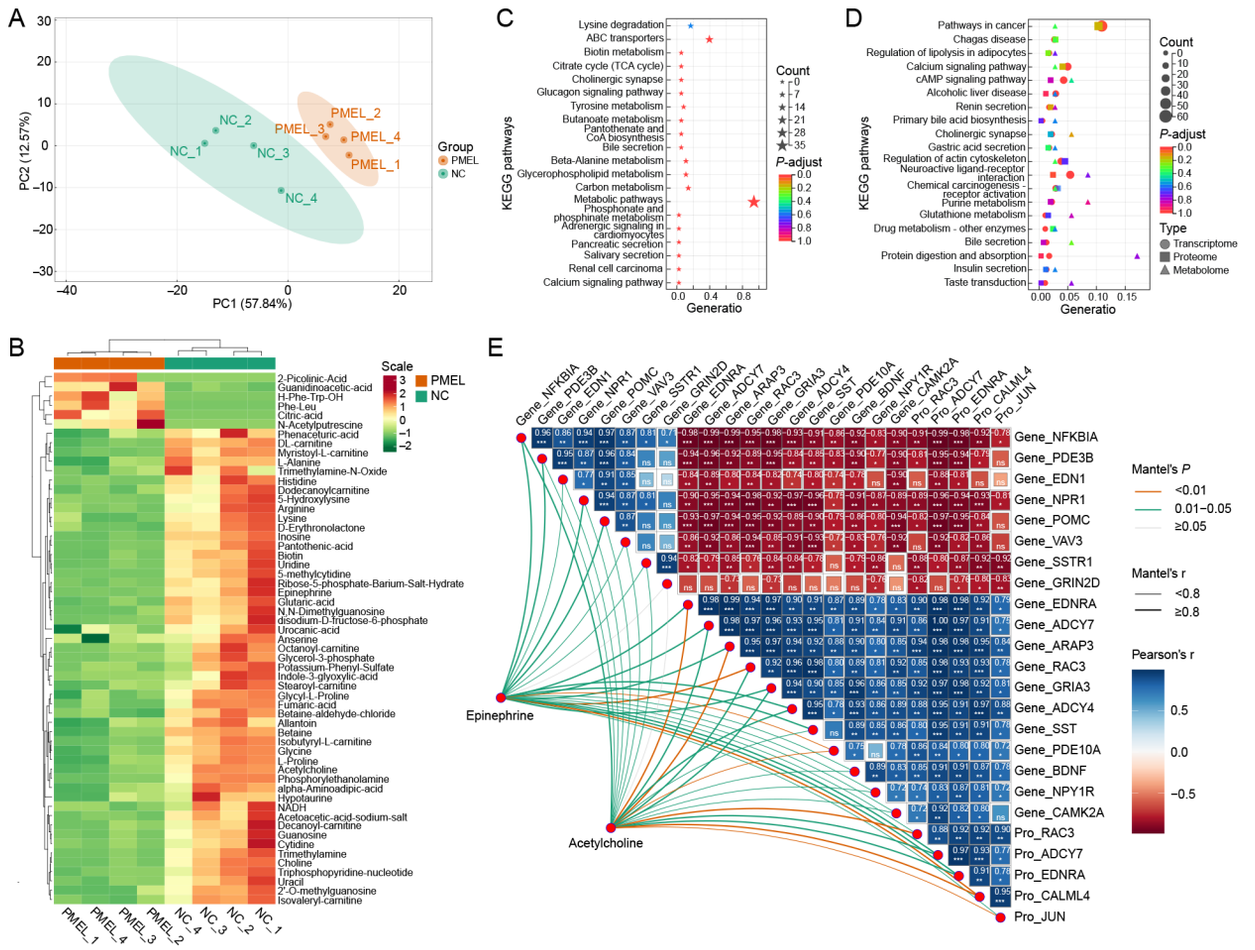

Figure 4 Metabolomic regulatory network of *PMEL* overexpression in yak fibroblasts (YFs)

A: PCA plot of samples from different groups. B: Heatmap of differentially expressed metabolites (DEMs) between groups. C: Top 20 KEGG pathways enriched by DEMs. D: KEGG pathways co-enriched by differentially expressed genes (DEGs), differentially expressed proteins (DEPs), and DEMs. E: Correlation analysis of DEGs, DEPs, and DEMs enriched in the cAMP signaling pathway. ns: Not significant; *: P<0.05; **: P<0.01; ***: P<0.001.

hypothesis that intronic variation in this locus may modulate transcriptional regulation, contributing to the molecular basis of coat color differentiation.

Fibroblasts modulate pigmentation by secreting a range of paracrine signals (e.g., *DKK1*, *NRG1*, and *FGF7*) that influence melanocyte differentiation, proliferation, and melanogenesis (Buac et al., 2009; Cardinali et al., 2005; Yamaguchi et al., 2004). In addition to their canonical signaling roles, fibroblasts have been shown to affect pigmentation through senescence-associated pathways (Kim et al., 2020) and, under reprogramming conditions, can transdifferentiate into functional melanocytes (Yang et al., 2014), highlighting their latent role in pigmentation pathways. Elucidating the regulatory network governing *PMEL* expression in YFs may thus provide critical insights into the genetic mechanisms underlying melanogenesis.

PMEL overexpression in YFs induced widespread transcriptional and proteomic remodeling, enriching key melanin- and pigmentation-related pathways. DEGs such as *OCA2*, *CAMK2A*, and *RAB38*, along with DEPs including RAB38, CALML4, and GADD45A, were implicated in pigment synthesis and regulation. *OCA2* is widely recognized as a critical gene in human pigmentation, with mutations such as rs7495174 T/C, rs6497268 G/T, and rs11855019 T/C leading to reduced melanin biosynthesis and severe depigmentation (Kamaraj & Purohit, 2014; Visser et al., 2014). Differential expression of *CAMK2A* has been linked to skin color variation in Wuzhishan pigs (Xu et al., 2019), while CALML4 has been implicated in melanogenesis in Xuefeng black-bone chickens (Deng et al., 2024). *RAB38* mediates vesicular trafficking of tyrosinase and other melanogenic enzymes (Wasmeier et al., 2006), a function critical for melanin synthesis. A missense mutation (p.Gly19Val) in *RAB38* disrupts this process, producing a brown coat in mice that phenocopies the pigmentation defect observed in TYRP1 mutants (Loftus et al., 2002). In parallel, GADD45A promotes apoptosis in melanoma cells through activation of the p38 MAPK pathway (Sarkar et al., 2002).

Overexpression of *PMEL* markedly suppressed the expression of neuregulin 1 (*NRG1*) and erb-b2 receptor tyrosine kinase 3 (*ERBB3*), key modulators of melanocyte behavior. *NRG1* facilitates melanocyte proliferation and influences pigmentation (Buac et al., 2009) by engaging *ERBB3* and *ERBB4* and inducing receptor dimerization, autophosphorylation, and activation of downstream signaling, such as the PI3K-Akt and MAPK cascade pathways (Ma et al., 2014; Zhang et al., 2013). These pathways are critical for melanocyte proliferation, differentiation, and survival (Zhang et al., 2013). Notably, *NRG1*/*ERBB3* signaling has been shown to inhibit melanocyte differentiation and pigment

production (Buac et al., 2009). In addition, several DEGs (e.g., *MAP2K6*, *FGF5*, and *FGFR3*) and DEPs (e.g., FGF7, JUN, and RAC3) were enriched in the Ras and MAPK signaling pathways, implicating *PMEL* in the regulation of fibroblast-derived signaling networks. *FGF7*, a paracrine factor secreted by fibroblasts, promotes melanosome transfer in keratinocytes (Liu et al., 2023) and activates both PI3K-Akt and Ras-Raf-MAPK pathways (Cardinali et al., 2005). *MAP2K6* drives the p38 MAPK axis (Kumar et al., 2021), while *RAC3* is required for p38 phosphorylation (Zhang et al., 2017), a key modulator of *CREB1* and *MITF* (Tagashira et al., 2015), which together orchestrate melanogenic transcriptional responses. *JUN*, a known driver of melanoma progression (Kappelmann-Fenzl et al., 2019), further links *PMEL*-associated proteomic changes to melanocyte transformation pathways.

PMEL overexpression also significantly down-regulated proopiomelanocortin (*POMC*) transcription. As a precursor for melanocortin peptides including α-MSH and ACTH, *POMC* regulates melanocyte-fibroblast crosstalk and melanocyte activation (Logesh et al., 2023; Slominski et al., 2004). α-MSH binds to *MC1R*, inducing adenylate cyclase activity (Rodríguez & Setaluri, 2014) and increasing intracellular cAMP via *ADCY4* and *ADCY7* (Chen et al., 2019; Joeyen-Waldorf et al., 2012). Elevated intracellular cAMP activates protein kinase A (Choi et al., 2022), which then transfers to the nucleus and phosphorylates CREB1, thereby enhancing *MITF* transcription (García-Borrón et al., 2014). cAMP also modulates PI3K-Akt signaling (Hu et al., 2022), with activated Akt phosphorylating glycogen synthase kinase 3β (*GSK3B*) at Ser9 (Choi et al., 2022), weakening its interaction with *MITF* and thereby promoting melanogenesis (Khaled et al., 2002).

Furthermore, overexpression of *PMEL* markedly reshaped the expression landscape of pigmentation-related genes (*ADCY7*, *EDN1*, and *EDNRA*) and proteins (FGF7, ADCY7, and EDNRA), which were predominantly enriched in the cAMP and PI3K-Akt signaling pathways. For instance, cAMP activation enhances FGF7 promoter activity (Finch et al., 1995), whereas FGF7 itself stimulates hair follicle growth and pigmentation via PI3K-Akt signaling (Lee et al., 2018; Pérez-Mora et al., 2023). The interaction between *EDN1* and its receptor *EDNRA* initiates MAPK and PI3K cascades that drive cellular proliferation, differentiation, and survival (Pulido et al., 2020) and is indispensable for melanocyte development, taurine metabolism, and hair regeneration (Bonano et al., 2008; Zhou et al., 2025). Moreover, PI3K-Akt signaling functions synergistically with Ras-Raf-MAPK to fine-tune melanocyte activity (Wang et al., 2017). Collectively, these findings indicate that *PMEL* influences melanin biosynthesis in YFs through integrated regulation of the cAMP/PI3K-Akt and Ras-Raf-MAPK signaling cascades.

Metabolomic analysis further revealed significant alterations in metabolites implicated in pigmentation regulation (Ferreira et al., 2023; Sonthalia et al., 2016). In this study, several DEMs, such as arginine, cytidine, and adrenaline, were enriched in ABC transporter and cAMP signaling pathways. Arginine depletion via arginine deiminase has been shown to suppress melanoma growth both *in vitro* and *in vivo* (Ensor et al., 2002), underscoring its metabolic relevance to pigmentation control. Cytidine reduces melanogenesis and melanosome transfer without affecting tyrosinase or DOPA oxidase activity (Diwakar et al., 2015), while betaine diminishes intracellular melanin accumulation by inhibiting tyrosinase activity and repressing *MITF* transcription in mouse melanocytes (Cho et al., 2017). Together, these molecular and metabolic alterations delineate a complex regulatory network through which *PMEL* modulates pigmentation at multiple biological levels.

Two metabolites, adrenaline and acetylcholine, enriched in the cAMP signaling pathway emerged as key modulators of melanogenesis. Epinephrine, a biologically active form of adrenaline, induces cAMP production via ADCY4, linking metabolic stimuli to second messenger signaling in pigment-producing cells (Chen et al., 2019). Acetylcholine, secreted by keratinocytes, modulates intracellular cAMP levels in adjacent melanocytes through muscarinic acetylcholine receptor signaling (Wu et al., 2018, 2020). Subsequently, intracellular cAMP regulates melanogenesis in melanocytes by influencing *MITF* expression (García-Borrón et al., 2014). Integrated multi-omics analyses revealed strong convergence within the cAMP axis, as evidenced by overlapping DEGs, DEPs, and DEMs. Acetylcholine, in particular, significantly downregulates MITF and TYR in B16F10 melanoma cells (Wu et al., 2018) and attenuates ultraviolet-induced melanogenesis in mice (Wu et al., 2020), underscoring its inhibitory role in pigment production. These findings highlight the complex interplay between metabolites and signaling pathways in regulating pigmentation.

Although this study established a robust association between *PMEL* and coat color variation in Sibu yaks, further empirical validation is necessary. Future investigations will increase the GWAS cohort size to strengthen the detection power and confirm the relevance of the lead SNP. Additionally, mechanistic studies in melanocytes will be conducted to dissect the regulatory role of *PMEL* in pigmentation pathways.

CONCLUSIONS

This study identified a strong correlation between *PMEL* gene variation (chr5: g.47487664 A>G) and yak coat color through GWAS and revealed significant differences in *PMEL* expression between brown and black Sibu YFs. Overexpression of *PMEL* influenced the expression of multiple pigmentation-related genes and metabolites, with the cAMP/PI3K-Akt and MAPK signaling pathways identified as key mediators of coat color development. These findings deepen our understanding of the genetic basis of coat color and provide valuable genetic markers for molecular breeding in yaks.

DATA AVAILABILITY

Raw data were deposited in the National Center for Biotechnology Information database (PRJNA1056509, PRJNA1064842), Genome Sequence Archive (https://ngdc.cncb.ac.cn/gsa, PRJCA042274, PRJCA042254), and Science Data Bank (https://www.scidb.cn/, 10.57760/sciencedb.27457, 10.57760/sciencedb.27398).

SUPPLEMENTARY DATA

Supplementary data to this article can be found online.

COMPETING INTERESTS

The authors declare that they have no competing interests

AUTHORS' CONTRIBUTIONS

Conceptualization: W.H.N., G.X.E., Q.Z.; Methodology: W.H.N., G.X.E.; Investigation: H.Y.Z., J.H.W.; Visualization: H.Y.Z., L.X., B.G.Y., C.L.L., P.C.R., T.R., H.C.; Resources: J.H.W., Q.Z., Y.Zhu, C.F.Z.; Formal

analysis: H.Y.Z.; Software: H.Y.Z., L.X., Funding acquisition: G.X.E., Q.Z.; Project administration: G.X.E., Q.Z., Y.Zhu, C.F.Z.; Supervision: Y.Zeng., S.C., S.Z.W., Y.G.H., Y.J.Z., Z.Q.Z., Y.F.H.; Writing – original draft: H.Y.Z.; Writing – review & editing: S.C., P.F.H., W.H.N., G.X.E. All authors read and approved the final version of the manuscript.

ACKNOWLEDGMENTS

We thank Da-Wei Yu and his team from the Institute of Animal Science, Chinese Academy of Agricultural Sciences, for providing the black and brown Sibu yak fibroblasts used in this study.

REFERENCES

Andersson LS, Wilbe M, Viluma A, et al. 2013. Equine multiple congenital ocular anomalies and silver coat colour result from the pleiotropic effects of mutant *PMEL*. *PLoS One*, **8**(9): e75639.

Ballif BC, Ramirez CJ, Carl CR, et al. 2018. The *PMEL* gene and merle in the domestic dog: a continuum of insertion lengths leads to a spectrum of coat color variations in Australian shepherds and related breeds. *Cytogenetic and Genome Research*, **156**(1): 22–34.

Baxter LL, Watkins-Chow DE, Pavan WJ, et al. 2019. A curated gene list for expanding the horizons of pigmentation biology. *Pigment Cell & Melanoma Research*, **32**(3): 348–358.

Bissig C, Rochin L, van Niel G. 2016. PMEL amyloid fibril formation: the bright steps of pigmentation. *International Journal of Molecular Sciences*, **17**(9): 1438.

Bonano M, Tríbulo C, De Calisto J, et al. 2008. A new role for the Endothelin-1/Endothelin-A receptor signaling during early neural crest specification. *Developmental Biology*, **323**(1): 114–129.

Bonaventure J, Domingues MJ, Larue L. 2013. Cellular and molecular mechanisms controlling the migration of melanocytes and melanoma cells. *Pigment Cell & Melanoma Research*, **26**(3): 316–325.

Brunberg E, Andersson L, Cothran G, et al. 2006. A missense mutation in *PMEL17* is associated with the Silver coat color in the horse. *BMC Genetics*, **7**: 46.

Buac K, Xu M, Cronin J, et al. 2009. NRG1 / ERBB3 signaling in melanocyte development and melanoma: inhibition of differentiation and promotion of proliferation. *Pigment Cell & Melanoma Research*, **22**(6): 773–784.

Cardinali G, Ceccarelli S, Kovacs D, et al. 2005. Keratinocyte growth factor promotes melanosome transfer to keratinocytes. *Journal of Investigative Dermatology*, **125**(6): 1190–1199.

Caro T, Mallarino R. 2020. Coloration in mammals. *Trends in Ecology & Evolution*, **35**(4): 357–366.

Chen RC, Zeng L, Zhu S, et al. 2019. cAMP metabolism controls caspase-11 inflammasome activation and pyroptosis in sepsis. *Science Advances*, **5**(5): eaav5562.

Cho BR, Jun HJ, Thach TT, et al. 2017. Betaine reduces cellular melanin content via suppression of microphthalmia-associated transcription factor in B16-F1 murine melanocytes. *Food Science and Biotechnology*, **26**(5): 1391–1397.

Choi H, Yoon JH, Youn K, et al. 2022. Decursin prevents melanogenesis by suppressing MITF expression through the regulation of PKA/CREB, MAPKs, and PI3K/Akt/GSK-3β cascades. *Biomedicine & Pharmacotherapy*, **147**: 112651.

Cieslak M, Reissmann M, Hofreiter M, et al. 2011. Colours of domestication. *Biological Reviews*, **86**(4): 885–899.

Correia MS, Moreiras H, Pereira FJC, et al. 2018. Melanin transferred to keratinocytes resides in nondegradative endocytic compartments. *Journal of Investigative Dermatology*, **138**(3): 637–646.

Cox J, Hein MY, Luber CA, et al. 2014. Accurate proteome-wide label-free quantification by delayed normalization and maximal peptide ratio extraction, termed MaxLFQ. *Molecular & Cellular Proteomics*, **13**(9): 2513–2526.

Deng YY, Qu XY, Yao YL, et al. 2024. Investigating the impact of pigmentation variation of breast muscle on growth traits, melanin deposition, and gene expression in Xuefeng black-bone chickens. *Poultry Science*, **103**(6): 103691.

Diwakar G, Klump V, Lazova R, et al. 2015. Evidence for glycosylation as a regulator of the pigmentary system: key roles of sialyl(α2-6)gal/GalNAc-terminated glycans in melanin synthesis and transfer. *Glycoconjugate Journal*, **32**(6): 413–420.

Du JY, Widlund HR, Horstmann MA, et al. 2004. Critical role of CDK2 for melanoma growth linked to its melanocyte-specific transcriptional regulation by MITF. *Cancer Cell*, **6**(6): 565–576.

Dun G, Li XL, Cao HZ, et al. 2007. Variations of melanocortin receptor 1 (*MC1R*) gene in three pig breeds. *Journal of Genetics and Genomics*, **34**(9): 777–782.

Edea Z, Dadi H, Dessie T, et al. 2018. Genome-wide scan reveals divergent selection among taurine and zebu cattle populations from different regions. *Animal Genetics*, **49**(6): 550–563.

Ensor CM, Holtsberg FW, Bomalaski JS, et al. 2002. Pegylated arginine deiminase (ADI-SS $PEG_{20,\ 000\ mw}$) inhibits human melanomas and hepatocellular carcinomas *in vitro* and *in vivo*. *Cancer Research*, **62**(19): 5443–5450.

Ferreira AM, de Souza AA, Koga RDCR, et al. 2023. Anti-melanogenic potential of natural and synthetic substances: application in zebrafish model. *Molecules*, **28**(3): 1053.

Finch PW, Lengel C, Chedid M. 1995. Cloning and characterization of the promoter region of the human keratinocyte growth factor gene. *Journal of Biological Chemistry*, **270**(19): 11230–11237.

Fontanesi L, Beretti F, Riggio V, et al. 2009. Missense and nonsense mutations in melanocortin 1 receptor (*MC1R*) gene of different goat breeds: association with red and black coat colour phenotypes but with unexpected evidences. *BMC Genetics*, **10**: 47.

Fontanesi L, D'Alessandro E, Scotti E, et al. 2010a. Genetic heterogeneity and selection signature at the *KIT* gene in pigs showing different coat colours and patterns. *Animal Genetics*, **41**(5): 478–492.

Fontanesi L, Tazzoli M, Russo V, et al. 2010b. Genetic heterogeneity at the bovine *KIT* gene in cattle breeds carrying different putative alleles at the *spotting* locus. *Animal Genetics*, **41**(3): 295–303.

Fowler DM, Koulov AV, Alory-Jost C, et al. 2006. Functional amyloid formation within mammalian tissue. *PLoS Biology*, **4**(1): e6.

Fullard JF, Giambartolomei C, Hauberg ME, et al. 2017. Open chromatin profiling of human postmortem brain infers functional roles for non-coding schizophrenia loci. *Human Molecular Genetics*, **26**(10): 1942–1951.

García-Borrón JC, Abdel-Malek Z, Jiménez-Cervantes C. 2014. MC1R, the cAMP pathway, and the response to solar UV: extending the horizon beyond pigmentation. *Pigment Cell & Melanoma Research*, **27**(5): 699–720.

Grabski DF, Broseus L, Kumari B, et al. 2021. Intron retention and its impact on gene expression and protein diversity: a review and a practical guide. *WIREs RNA*, **12**(1): e1631.

Guo JZ, Sun XL, Mao AY, et al. 2022. A 13.42-kb tandem duplication at the *ASIP* locus is strongly associated with the depigmentation phenotype of non-classic Swiss markings in goats. *BMC Genomics*, **23**(1): 437.

Guo Z, Boekhoudt GH, Boss JM. 2003. Role of the intronic enhancer in tumor necrosis factor-mediated induction of manganous superoxide dismutase. *Journal of Biological Chemistry*, **278**(26): 23570–23578.

He YM, Huang YF, Wang SZ, et al. 2022. Hereditary basis of coat color and excellent feed conversion rate of red angus cattle by next-generation sequencing data. *Animals*, **12**(12): 1509.

Hellström AR, Watt B, Fard SS, et al. 2011. Inactivation of *Pmel* alters melanosome shape but has only a subtle effect on visible pigmentation.

PLoS Genetics, **7**(9): e1002285.

Hu YB, Chen Y, Zhao Y, et al. 2023. Tranexamic acid may promote melanocores clustering in keratinocytes through upregulation of Rab5b. *Experimental Dermatology*, **32**(6): 777–786.

Hu ZZ, Sha XM, Zhang L, et al. 2022. Effect of grass carp scale collagen peptide FTGML on cAMP-PI3K/Akt and MAPK signaling pathways in B16F10 melanoma cells and correlation between anti-melanin and antioxidant properties. *Foods*, **11**(3): 391.

Ji QM, Xin JW, Chai ZX, et al. 2021. A chromosome-scale reference genome and genome-wide genetic variations elucidate adaptation in yak. *Molecular Ecology Resources*, **21**(1): 201–211.

Jiang LD, Zheng ZL, Fang HL, et al. 2021. A generalized linear mixed model association tool for biobank-scale data. *Nature Genetics*, **53**(11): 1616–1621.

Joeyen-Waldorf J, Nikolova YS, Edgar N, et al. 2012. Adenylate cyclase 7 is implicated in the biology of depression and modulation of affective neural circuitry. *Biological Psychiatry*, **71**(7): 627–632.

Kamaraj B, Purohit R. 2014. Computational screening of disease-associated mutations in OCA2 gene. *Cell Biochemistry and Biophysics*, **68**(1): 97–109.

Kappelmann-Fenzl M, Gebhard C, Matthies AO, et al. 2019. *C-Jun* drives melanoma progression in *PTEN* wild type melanoma cells. *Cell Death & Disease*, **10**(8): 584.

Khaled M, Larribere L, Bille K, et al. 2002. Glycogen synthase kinase 3β is activated by cAMP and plays an active role in the regulation of melanogenesis. *Journal of Biological Chemistry*, **277**(37): 33690–33697.

Kim Y, Kang B, Kim JC, et al. 2020. Senescent fibroblast-derived GDF15 induces skin pigmentation. *Journal of Investigative Dermatology*, **140**(12): 2478–2486. e4.

Kimura S, Hatakeyama T, Koutaka T, et al. 2022. *PMEL* p. Leu18del dilutes coat color of Kumamoto sub-breed of Japanese Brown cattle. *BMC Genomics*, **23**(1): 694.

Kumar GS, Page R, Peti W. 2021. The interaction of p38 with its upstream kinase MKK6. *Protein Science*, **30**(4): 908–913.

Kwon BS, Halaban R, Ponnazhagan S, et al. 1995. Mouse *silver* mutation is caused by a single base insertion in the putative cytoplasmic domain of Pmel 17. *Nucleic Acids Research*, **23**(1): 154–158.

Lambert MW, Maddukuri S, Karanfilian KM, et al. 2019. The physiology of melanin deposition in health and disease. *Clinics in Dermatology*, **37**(5): 402–417.

Lan DL, Ji WH, Xiong XR, et al. 2021. Population genome of the newly discovered Jinchuan yak to understand its adaptive evolution in extreme environments and generation mechanism of the multirib trait. *Integrative Zoology*, **16**(5): 685–695.

Larsen BM, Cowan JE, Wang YQ, et al. 2019. Identification of an intronic regulatory element necessary for tissue-specific expression of *Foxn1* in thymic epithelial cells. *The Journal of Immunology*, **203**(3): 686–695.

Le L, Sirés-Campos J, Raposo G, et al. 2021. Melanosome biogenesis in the pigmentation of mammalian skin. *Integrative and Comparative Biology*, **61**(4): 1517–1545.

Lee CY, Yang CY, Lin CC, et al. 2018. Hair growth is promoted by BeauTop via expression of EGF and FGF-7. *Molecular Medicine Reports*, **17**(6): 8047–8052.

Liu Q, Huang JY, Yan WW, et al. 2023. FGFR families: biological functions and therapeutic interventions in tumors. *MedComm*, **4**(5): e367.

Loftus SK, Larson DM, Baxter LL, et al. 2002. Mutation of melanosome protein RAB38 in *chocolate* mice. *Proceedings of the National Academy of Sciences of the United States of America*, **99**(7): 4471–4476.

Logesh R, Prasad SR, Chipurupalli S, et al. 2023. Natural tyrosinase enzyme inhibitors: a path from melanin to melanoma and its reported pharmacological activities. *Biochimica et Biophysica Acta (BBA) - Reviews on Cancer*, **1878**(6): 188968.

Ma J, Lyu H, Huang JC, et al. 2014. Targeting of erbB3 receptor to overcome resistance in cancer treatment. *Molecular Cancer*, **13**: 105.

Ma XM, Jia CJ, Fu DH, et al. 2019. Analysis of hematological traits in polled yak by genome-wide association studies using individual SNPs and haplotypes. *Genes*, **10**(6): 463.

Mun Y, Kim W, Shin D. 2023. Melanocortin 1 receptor (MC1R): pharmacological and therapeutic aspects. *International Journal of Molecular Sciences*, **24**(15): 12152.

Norris BJ, Whan VA. 2008. A gene duplication affecting expression of the ovine *ASIP* gene is responsible for white and black sheep. *Genome Research*, **18**(8): 1282–1293.

Pérez-Mora S, Ocampo-López J, Gómez-García MDC, et al. 2023. BFNB enhances hair growth in C57BL/6 mice through the induction of EGF and FGF7 factors and the PI3K-AKT-β-catenin pathway. *International Journal of Molecular Sciences*, **24**(15): 12110.

Pulido I, Ollosi S, Aparisi S, et al. 2020. Endothelin-1-mediated drug resistance in *EGFR*-mutant non-small cell lung carcinoma. *Cancer Research*, **80**(19): 4224–4232.

Ren J, Mao H, Zhang Z, et al. 2011. A 6-bp deletion in the *TYRP1* gene causes the brown colouration phenotype in Chinese indigenous pigs. *Heredity*, **106**(5): 862–868.

Rodríguez CI, Setaluri V. 2014. Cyclic AMP (cAMP) signaling in melanocytes and melanoma. *Archives of Biochemistry and Biophysics*, **563**: 22–27.

Sarkar D, Su ZZ, Lebedeva IV, et al. 2002. *mda*-7 (IL-24) mediates selective apoptosis in human melanoma cells by inducing the coordinated overexpression of the GADD family of genes by means of p38 MAPK. *Proceedings of the National Academy of Sciences of the United States of America*, **99**(15): 10054–10059.

Shaul O. 2017. How introns enhance gene expression. *The International Journal of Biochemistry & Cell Biology*, **91**: 145–155.

Slominski A, Tobin DJ, Shibahara S, et al. 2004. Melanin pigmentation in mammalian skin and its hormonal regulation. *Physiological Reviews*, **84**(4): 1155–1228.

Sonthalia S, Daulatabad D, Sarkar R. 2016. Glutathione as a skin whitening agent: facts, myths, evidence and controversies. *Indian Journal of Dermatology, Venereology and Leprology*, **82**(3): 262–272.

Sun LJ, Hu L, Zhang P, et al. 2018. Silencing of PMEL attenuates melanization via activating lysosomes and degradation of tyrosinase by lysosomes. *Biochemical and Biophysical Research Communications*, **503**(4): 2536–2542.

Sun PY, Zhang GY, Xian M, et al. 2023. Proteomic analysis of frozen-thawed spermatozoa with different levels of freezability in dairy goats. *International Journal of Molecular Sciences*, **24**(21): 15550.

Tagashira H, Miyamoto A, Kitamura SI, et al. 2015. UVB stimulates the expression of endothelin B receptor in human melanocytes via a sequential activation of the p38/MSK1/CREB/MITF pathway which can be interrupted by a French maritime pine bark extract through a direct inactivation of MSK1. *PLoS One*, **10**(6): e0128678.

Trigo BB, Utsunomiya ATH, Fortunato AAAD, et al. 2021. Variants at the *ASIP* locus contribute to coat color darkening in Nellore cattle. *Genetics Selection Evolution*, **53**(1): 40.

Visser M, Kayser M, Grosveld F, et al. 2014. Genetic variation in regulatory DNA elements: the case of *OCA2* transcriptional regulation. *Pigment Cell & Melanoma Research*, **27**(2): 169–177.

Visser M, Palstra RJ, Kayser M. 2015. Allele-specific transcriptional regulation of *IRF4* in melanocytes is mediated by chromatin looping of the intronic rs12203592 enhancer to the *IRF4* promoter. *Human Molecular Genetics*, **24**(9): 2649–2661.

Voisey J, Van Daal A. 2002. Agouti: from mouse to man, from skin to fat.

Pigment Cell Research, **15**(1): 10–18.

Wang J, Fan TT, Du ZW, et al. 2023. Genome-wide association analysis identifies the PMEL gene affecting coat color and birth weight in Simmental × Holstein. *Animals*, **13**(24): 3821.

Wang JB, Chai ZX, Deng L, et al. 2020. Detection and integrated analysis of lncRNA and mRNA relevant to plateau adaptation of Yak. *Reproduction in Domestic Animals*, **55**(11): 1461–1469.

Wang YJ, Viennet C, Robin S, et al. 2017. Precise role of dermal fibroblasts on melanocyte pigmentation. *Journal of Dermatological Science*, **88**(2): 159–166.

Ward LD, Kellis M. 2012. Interpreting noncoding genetic variation in complex traits and human disease. *Nature Biotechnology*, **30**(11): 1095–1106.

Wasmeier C, Romao M, Plowright L, et al. 2006. Rab38 and Rab32 control post-Golgi trafficking of melanogenic enzymes. *The Journal of Cell Biology*, **175**(2): 271–281.

Weiner L, Fu WY, Chirico WJ, et al. 2014. Skin as a living coloring book: how epithelial cells create patterns of pigmentation. *Pigment Cell & Melanoma Research*, **27**(6): 1014–1031.

Wu QY, Fung AHY, Xu ML, et al. 2018. Microphthalmia-associated transcription factor up-regulates acetylcholinesterase expression during melanogenesis of murine melanoma cells. *Journal of Biological Chemistry*, **293**(37): 14417–14428.

Wu QY, Xia YT, Dai K, et al. 2020. Solar light induces the release of acetylcholine from skin keratinocytes affecting melanogenesis. *The FASEB Journal*, **34**(7): 8941–8958.

Xiang GH, Ren JL, Hai T, et al. 2018. Editing porcine *IGF2* regulatory element improved meat production in Chinese Bama pigs. *Cellular and Molecular Life Sciences*, **75**(24): 4619–4628.

Xu Q, Liu XM, Chao Z, et al. 2019. Transcriptomic analysis of coding genes and non-coding RNAs reveals complex regulatory networks underlying the black back and white belly coat phenotype in Chinese Wuzhishan pigs. *Genes*, **10**(3): 201.

Yamaguchi Y, Itami S, Watabe H, et al. 2004. Mesenchymal-epithelial interactions in the skin: increased expression of dickkopf1 by palmoplantar fibroblasts inhibits melanocyte growth and differentiation. *The Journal of Cell Biology*, **165**(2): 275–285.

Yang GL, Fu DL, Lang X, et al. 2013. Mutations in *MC1R* gene determine black coat color phenotype in Chinese sheep. *The Scientific World Journal*, **2013**: 675382.

Yang RF, Zheng Y, Li L, et al. 2014. Direct conversion of mouse and human fibroblasts to functional melanocytes by defined factors. *Nature Communications*, **5**: 5807.

Zhang CL, Liu TQ, Wang GB, et al. 2017. Rac3 regulates cell invasion, migration and EMT in lung adenocarcinoma through p38 MAPK pathway. *Journal of Cancer*, **8**(13): 2511–2522.

Zhang FW, Wang C, Xu HY, et al. 2023. Genomic analysis reveals a *KIT*-related chromosomal translocation associated with the white coat phenotype in yak. *Journal of Animal Breeding and Genetics*, **140**(3): 330–342.

Zhang J, Wang C, Liu Y, et al. 2016. Agouti signalling protein (*ASIP*) gene: molecular cloning, sequence characterisation and tissue distribution in domestic goose. *British Poultry Science*, **57**(3): 288–294.

Zhang KM, Wong P, Duan JQ, et al. 2013. An ERBB3/ERBB2 oncogenic unit plays a key role in NRG1 signaling and melanoma cell growth and survival. *Pigment Cell & Melanoma Research*, **26**(3): 408–414.

Zhang MQ, Xu X, Luo SJ. 2014. The genetics of brown coat color and white spotting in domestic yaks (*Bos grunniens*). *Animal Genetics*, **45**(5): 652–659.

Zhou SY, Li ZM, Li XZ, et al. 2025. Crosstalk between endothelial cells and dermal papilla entails hair regeneration and angiogenesis during aging. *Journal of Advanced Research*, **70**: 339–353.